VLBA Observations of G5.89-0.39: OH masers and magnetic field structure

D.P. Stark[1,3], W.M. Goss[2], E. Churchwell [3], V.L. Fish [2,5], I. M. Hoffman [4]

ABSTRACT

We present VLBA observations of 1667 MHz OH maser emission from the massive star formation region G5.89-0.39. The observations were phase referenced allowing the absolute positions of the masers to be obtained. The 1667 MHz masers have radial velocities that span ∼50 km s^{-1} but show little evidence of tracing the bipolar molecular outflow, as has been claimed in previous studies. We identify 23 Zeeman pairs through comparison of masers in left and right circular polarization. Magnetic field strengths range from −2 mG to +2 mG, and an ordered reversal in magnetic field direction is observed toward the southern region of the UC HII region. We suggest that the velocity and magnetic field structure of the 1667 MHz masers can be explained in the context of a model in which the masers arise in a neutral shell just outside a rapidly exanding ionized shell.

Subject headings: HII regions – ISM: individual (G5.89-0.39) magnetic fields – masers – stars: formation

1. Introduction

Massive stars are born in optically thick, dense molecular clouds. Since optical emission from young embedded massive stars is completely absorbed by surrounding gas and dust, other means must be used to identify the formation process of massive stars; hence, massive

[1]Department of Astronomy, California Institute of Technology, MS 105-24, Pasadena, CA 91125; dps@astro.caltech.edu

[2]National Radio Astronomy Observatory, P.O. Box 0, 1003 Lopezville Road, Socorro, NM 87801

[3]Astronomy Department, University of Wisconsin, 475 N. Charter St., Madison, WI 53706

[4]St. Paul's School, 325 Pleasant Street, Concord, NH 03301

[5]Jansky Fellow

star formation regions are often identified by one or more of the following: ultra-compact regions of ionized hydrogen (UC HII regions), powerful molecular outflows, and strong molecular masers. Studies of maser emission toward star formation regions offer several advantages. The high intensity and small spatial scales of maser spots allow star formation regions to be probed on scales $\gtrsim 10^{14}$ cm, providing an effective method of studying the kinematics of gas associated with forming stars. Furthermore, Zeeman splitting of maser lines provides information about the magnetic field structure of molecular gas surrounding young massive stars, offering the possibility to clarify the role of magnetic fields in the collimation of bipolar outflows of massive stars.

In many of the regions for which hydroxyl (hereafter OH) masers have been studied in detail, their velocity structure and distribution suggests that they trace a dense disk or molecular torus (Hutawarakorn & Cohen 1999; Hutawarakorn et al. 2002; Hutawarakorn & Cohen 2003, 2005). The magnetic field structure in these regions typically shows a toroidal component reversing directions on either side of the disk which appears to support the model in which magnetic field lines are twisted by the rotating disk (Uchida & Shibata 1985).

A case where the main-line OH masers are predicted to instead trace the bipolar outflow is toward the massive star formation region G5.89-0.39 (GAL 005.886-00.393 in SIMBAD and hereafter referred to as G5.89). G5.89 is a shell-like UC HII region, powered by a young massive star of spectral type O6 or O7 (Wood & Churchwell 1989). A dense ($n_{H_2}\sim10^4$ cm^{-3}), hot (T$\sim$90 K), and massive (M$\sim$30 M$_\odot$) envelope of dust and molecular gas surrounds the ionized gas (Gomez et al. 1991; Harvey et al. 1994) and appears to be participating in a powerful bipolar molecular outflow (Harvey & Forveille 1988; Cesaroni et al. 1991; Zijlstra et al. 1990; Acord et al. 1997; Sollins et al. 2004; Watson 2004). Proper motion observations of the expansion velocity of G5.89 suggest a distance of $\simeq$2 kpc (Acord et al. 1998). More recently, the distance to G5.89 has been estimated kinematically by Fish et al. (2003) using HI absorption features to resolve the near/far kinematic ambiguity. The inferred distance of $\simeq$3.8 kpc is consistent with the Acord et al. (1998) estimate within the quoted error bars. Nevertheless, we adopt the Acord et al. (1998) distance estimate because the kinematic distance method has large uncertainties for sources located near a galactic longitude of $\simeq0^\circ$. Observations of radio recombination lines suggest an LSR velocity of $\simeq$ 10 km s^{-1} (Reifenstein et al. 1970; Wood & Churchwell 1989) which we assume to be the systemic velocity of G5.89.

OH maser emission was detected toward G5.89 with the Very Large Array (VLA) by Zijlstra et al. (1990) at 1612 MHz, 1665 MHz, and 1667 MHz. Main-line OH maser spectra in other sources typically show many components spanning a range of $\sim$10 km s^{-1} in radial velocity; toward G5.89, OH maser emission spans a range $\simeq$50 km s^{-1}. The 1667 MHz

maser features extend primarily N-S, perpendicular to a disk-like structure inferred from the morphology of the 6 cm continuum emission. The radial velocities of the masers increase with distance away from the disk-like structure. (Zijlstra et al. 1990) suggest that the main-line OH masers observed toward G5.89 trace an accelerating component of the bipolar molecular outflow. If this interpretation is valid, identification of Zeeman pairs could yield the magnetic field structure along the outflow, allowing valuable constraints to be placed on hydromagnetic models for bipolar outflows (Shu et al. 1994).

Recent observations indicate that such an interpretation may require closer scrutiny. The outflow position angle differs considerably depending on the tracer, ranging from NE-SW in SiO(5-4) (Sollins et al. 2004), to N-S as traced by $C^{34}S$ (Cesaroni et al. 1991) to E-W (and primarily along the line-of-sight) as traced by CO(1-0) and HCO^+ (Watson 2004). The source of the outflow has also been debated. Feldt et al. (2003) detect an O5 star slightly offset from the center of the UC HII region and suggest that this object may be the ionizing source of G5.89. Sollins et al. (2004) argue that the outflow is likely not powered by the O5 star since the star is not equidistant from the outflow lobes, but rather originates from the 1.3 mm continuum source detected in their work. However, they cannot distinguish whether the 1.3 mm continuum emission is associated with the UC HII region. Studying the maser emission with the spatial resolution offered by very long baseline interferometry could help clarify these uncertainties.

Since the work of Zijlstra et al. (1990), there have been several new studies of main-line OH maser emission toward G5.89. Wood (1993) and Argon et al. (2000) observed 1665 MHz and 1667 MHz OH masers with the VLA in left circular polarization (LCP) and right circular polarization (RCP). The angular resolution of the Wood (1993) and Argon et al. (2000) observations was $\simeq 2''$ compared to the $6''$ resolution achieved by Zijlstra et al. (1990); however, even with $2''$ resolution, it is not possible to reliably identify Zeeman pairs. Fish et al. (2005) identify Zeeman pairs toward G5.89 using 1665 MHz and 1667 MHz OH masers with the VLBA, but their observations only cover a fraction of the velocity-range in which OH masers are known to reside.

In an attempt to 1) explore the velocity structure of the gas traced by the OH masers and 2) characterize the magnetic field of molecular gas surrounding G5.89, we have observed the 1667 MHz and 1612 MHz OH maser lines toward G5.89 with the Very Long Baseline Array (VLBA) of the NRAO[1]. The angular resolution ($\sim$10 milliarcsecs) and spectral resolution ($\simeq$0.2 km s^{-1} at 1612 and 1667 MHz) are sufficient to identify the location of OH maser

[1]The National Radio Astronomy Observatory (NRAO) is a facility of the National Science Foundation operated under cooperative agreement by Associated Universities, Inc.

clumps and identify Zeeman pairs. The observations and reduction techniques are presented in §2. In §3 and §4, we present and discuss the results of our OH maser observations toward G5.89. Finally, in §5, the results are summarized.

2. Observations

The 1667.35903 MHz (hereafter 1667 MHz) and 1612.23101 MHz (hereafter 1612 MHz) transitions were observed toward G5.89 with the VLBA on 2003 May 13-14. Left and right circular polarizations were observed simultaneously in 1024 spectral channels covering a total bandwidth of 1.0 MHz resulting in a channel width of 0.176 km s^{-1} at 1667 MHz and 0.182 km s^{-1} at 1612 MHz. At 1667 MHz, only those channels with emission (500-700) were imaged. The resulting velocity resolution (1.2 times the channel separation) was 0.218 km s^{-1} at 1667 MHz and 0.211 km s^{-1} at 1612 MHz.

Calibrations and imaging were performed with the NRAO AIPS[2] software package. Amplitudes were calibrated using on-line system noise temperature and gain curves. Delay and bandpass response solutions were found via three scans of the compact continuum source 3C 345. The maser observations were phase referenced to J1751-2524 (offset 1.3 degrees from G5.89) using a cycle time of 6 minutes (3 minutes on G5.89, 3 minutes on J1751-2524). This source has a flux density of 0.67 Jy in the S-band and a positional error of 2.5 mas. The uncertainty in the absolute position of bright ($\simeq$1 Jy) maser spots is thus $\sim$3 mas.

A single bright maser spot in each maser transition and polarization was selected for self-calibration in each maser transition and polarization. Interstellar scatter broadening causes the self-calibration sources to become resolved on the longer baselines of the VLBA, significantly reducing the signal to noise and causing the calibration to fail on these baselines. The maser used for self-calibration at 1612 MHz was brighter than that at 1667 MHz allowing three more antennas to be calibrated at 1612 MHz. The long baselines available from the three extra antennas result in a significantly smaller synthesized beam at 1612 MHz. The resulting synthesized beams of the 1612 MHz and 1667 MHz images are 20 $\times$ 7 mas at a position angle of 7° and 45 $\times$ 15 mas with a 27° position angle, respectively. At the distance of G5.89, this corresponds to $\simeq$30 AU at 1612 MHz and $\simeq$50 AU at 1667 MHz. The rms noise of the cleaned image is 129 mJy $beam^{-1}$ at 1612 MHz and 49 mJy $beam^{-1}$ at 1667 MHz. The observations cover a field 8.2 $\times$ 8.2 $arcsec^2$ centered on α_{J2000}=18^h $00^m30\overset{s}{.}382$ δ_{J2000}=−24°04'00$\overset{''}{.}$829. Details of the observations and instrumental characteristics are presented in Table 1.

[2]The Astronomical Image Processing System (AIPS) is documented at http ://www.nrao.edu/aips

Using the task JMFIT in AIPS, two-dimensional Gaussians were fit to all peaks detected in adjacent channels with significance above 5σ to identify and calculate the flux density of each maser spot. Line profiles were fit using IDL software routines. Maser positions, flux densities, and velocities are listed in Table 2 (1667 MHZ LCP), Table 3 (1667 MHZ RCP), and Table 4 (1612 MHz). The maser velocities listed in these tables are not corrected for the shift induced by the Zeeman effect.

3. Results

3.1. Maser Properties, Position, and Velocity Structure

Fifty-nine maser spots were identified in LCP and fifty-five in RCP at 1667 MHz with velocities ranging from -32.13 km s^{-1} to $+15.30$ km s^{-1}. Figures 1-2 display the positions of the LCP and RCP masers, respectively, relative to the VLA 8.5 GHz radio continuum image (Churchwell 2003, private communication) . The offset between the masers and radio continuum emission is only known at the level of $\simeq 0\farcs3$ (Argon et al. 2000), however the absolute positions of the masers are known at the level of a few mas since they are phase referenced. For ease of discussion, we subdivide the OH maser features into three groups projected on 1) the S-edge of the UC HII (hereafter, G5.89 South) and 2) the E-edge of the UC HII region (G5.89 East) and 3) the center of the UC HII region (G5.89 Center). We zoom in on the distribution of masers in the center of G5.89 in Figure 3 and in the south of G5.89 in Figure 4. In Figures 5, 6, and 7 we plot spectra of 1667 MHz averaged over G5.89 South, G5.89 East, and G5.89 Center, respectively. The velocities of maser features on the edges of the UC HII region are positive and close to the systemic velocity of 10 km s^{-1}, whereas the velocities of masers projected on the center of the UC HII region are blueshifted by up to 40 km s^{-1} with respect to the systemic velocity. In § 4, we will explain this observation as an optical depth effect.

At 1612 MHz, we observed three masers in both LCP and RCP. The positions of 1612 MHz OH masers are presented in Table 4, Figure 8 (LCP), and Figure 9 (RCP). The masers are projected on the central region of the UC HII region and their line-of-sight velocities are $\simeq -20$ km s^{-1}. Zijlstra et al. (1990) identify 1612 MHz OH masers with roughly the same projected position and line-of-sight velocity. They also identify several weaker masers at $\simeq$10 km s^{-1} projected on the southern region of the UC HII region which are outside our velocity coverage and hence not detected in our observations. The -20 km s^{-1} component was first observed by Turner (1969). As with Zijlstra et al. (1990), we find that this line is divided in several components. While the ratio of flux densities between the different components appears to have varied in the fifteen years between the Zijlstra et al. (1990)

VLA observations from 1988 and the 2003 VLBA observations that make up this work, quantifying the variability is complicated by the different resolutions of the VLA and VLBA.

The median deconvolved major axis of the 1667 MHz masers is 16 mas in LCP and 17 mas in RCP; both values are roughly consistent with the previous measurement of 20 mas in Fish & Reid (2006). At 1612 MHz, the median deconvolved major axis is 20 mas in LCP and 21 mas in RCP. This suggests that many of the 1667 MHz and 1612 MHZ masers may be partially resolved. However, we note that the deconvolved spot parameters may overestimate the true spot size (Fish & Reid 2006), in part due to scatter broadening.

The OH maser observations presented in this paper were conducted two years after the observations of Fish et al. (2005). Given the large radial velocities of the masers relative to the assumed systemic velocity of the system, it is worthwhile to examine whether there is a positional displacement between the maser spots observed at 1667 MHz by Fish et al. (2005) and those presented in this paper. The data presented in Fish et al. (2005) were not phase referenced so the absolute positions of the masers are unknown. However, the relative positions are known to very high precision, allowing the relative proper motions of masers to be studied. Since Fish et al. (2005) only observe positive velocity features, we are limited to a subset of the masers presented in this paper. We identified twelve LCP and eleven RCP masers in common between the two datasets. The relative proper motions are derived by comparing the relative displacement between these maser features in Fish et al. (2005) to those in this paper; if the masers tangential velocities are large, then we would expect the relative displacements to differ between the two epochs. The relative angular displacement between masers in G5.89-E and G5.89-S increases by 5-6 mas between the two epochs. At the distance of G5.89, this proper motion corresponds to 20-30 km s^{-1}. There is also significant relative proper motions ($\gtrsim$4 mas) between the individual masers in G5.89 S indicating that these masers may be moving at speeds of $\gtrsim$20 km s^{-1} with respect to one another.

3.2. Magnetic Field Structure

A catalog of Zeeman pairs was created by identifying all LCP and RCP lines that are separated on the sky by less than $\simeq$90 AU, comparable to the size of our synthesized beam at the distance of G5.89. Observations of W3(OH) (Reid et al. 1980) suggest that this distance requirement is sufficiently rigorous to reliably derive the magnetic field. We only classify masers as Zeeman pairs if the velocity centroiding error of the pair is less than twice the velocity offset between polarizations, where we have taken the velocity centroiding error to be the quadrature sum of the fitted half-width half maximum divided by twice the signal to

noise ratio of the lines. The magnetic field strength is directly related to the velocity offset between the LCP and RCP components: B = (Δv/0.354 km s^{-1}) mG at 1667 MHz and B = (Δv/0.120 km s^{-1}) mG at 1612 MHz. A positive line-of-sight magnetic field (i.e. oriented away from the Earth) is assigned to those Zeeman pairs with $v_{RCP} > v_{LCP}$, and a negative magnetic field is assigned to those with $v_{LCP} > v_{RCP}$.

Following the method of Hutawarakorn & Cohen (2003), we estimate a $\lesssim$ 1.4, 2.0, 6.2 % probability that any of the Zeeman pairs identified in G5.89 East, Center, and South are due to random spatial overlap of components of opposite polarization. The probability is found by dividing the number of possible pairs in a given region (using the same selection criteria as described above) by the total area of that region and then multiplying by the maximum area of separation over which two masers of opposite polarization are identified as Zeeman pairs (the synthesized beam area). The reasonably low probability suggests that the Zeeman pairs in this sample are not likely to be false detections.

We find 23 Zeeman pairs in our sample of 1667 MHz masers. Properties of the pairs are summarized in Table 5. All maser velocities quoted in the text and figures of this section are corrected for the Zeeman effect. Spectra of two Zeeman pairs from our observations are displayed in Figure 10. The velocity offset between the LCP and RCP spectra is clearly visible in both spectra. In the bottom panel, the flux density of the LCP component is lower than that in RCP. This effect is commonly observed in other massive star formation regions (Moran et al. 1978) and perhaps is a result of velocity or magnetic field gradients causing differential gain for masers of opposite polarizations (Cook 1968). In a more extreme case, the differential amplification between polarizations may result in a maser line being above the detection threshold in only one polarization, perhaps explaining why just over half of the masers in our survey have identifiable Zeeman pairs.

In Figure 11, we overlay the positions of the Zeeman pairs on the 8.5 GHz continuum image. Negative line-of-sight magnetic field strengths are denoted with circles while positive line-of-sight magnetic field strenghs are denoted with crosses. Magnetic field strengths vary from -1.97 mG to $+1.94$ mG across the field of G5.89.

The polarity of the field is positive for all three pairs detected in the E group. Two of the pairs are part of a clump of negative velocity features (-14.96 and -16.43 km s $^{-1}$) with projected separation of only 75 mas, implying typical linear separations of $\sim$150 AU. The corresponding line-of-sight magnetic field strengths are 0.52 mG and 1.34 mG. The third Zeeman pair in the east group is offset 770 mas E of the other pairs. The line-of-sight velocity of the pair, 10.03 km s^{-1} is significantly offset from velocities of the other two pairs in the region, while the line-of-sight magnetic field strength, 1.41 mG, is comparable in strength and sign to the other pairs.

Eleven Zeeman pairs are found projected on the central region with velocities ranging between -31.32 km s^{-1} and -18.74 km s^{-1}. The radial velocities of most of the pairs in this region are centered closely around the median velocity of -25.45 km s^{-1}. The magnetic field polarity is positive for all but two of the Zeeman pairs, with amplitudes ranging from 0.28 mG to 1.49 mG.

The field structure derived from the eleven Zeeman pairs in the S group is more complex than the two previously discussed regions. The two southernmost Zeeman pairs have radial velocities ranging from 13.01 km s^{-1} to 13.91 km s^{-1} and line-of-sight magnetic fields of negative polarity. Also in the S group is a collection of nine Zeeman pairs which display an ordered reversal in magnetic field polarity over 300 mas, roughly $\sim$600 AU at the distance of G5.89. Such field reversals may arise if OH masers trace a rotating molecular torus (Hutawarakorn & Cohen 1999; Hutawarakorn et al. 2002; Hutawarakorn & Cohen 2003, 2005). In this scenario, the field lines are thought to become entrained in the torus producing the observed toroidal component. This does not appear to be the case toward G5.89 because the the velocity structure does not vary in an ordered fashion across the gas traced by the Zeeman pairs (Figure 12). Pairs with negative field polarity have velocities ranging from -29.04 to -18.04 km s^{-1} while those with positive field polarity have velocities ranging from -22.08 to -18.74 km s^{-1}. Not only do the velocities of the pairs not vary systematically with position, but they also trace gas that is moving at $\simeq$30 km s^{-1} with respect to LSR velocity of G5.89. Hence, we find no indication of rotation in this clump of maser emission.

We find good agreement between the magnetic field structure we present in Figure 11 with that presented in Fish et al. (2005). In the E-group, Fish et al. (2005) identify 4 pairs at 1667 MHz; similar to our observations, all pairs have positive magnetic field polarity with a median field strength of 1.5 mG. In G5.89-S, Fish et al. (2005) identify 3 pairs that appear to be part of the same clump of masers we observe in the south of the region. The field direction is negative for all pairs in this region, with a median field strength of -1.5 mG; both measurements are consistent with the observations presented in this paper. Fish et al. (2005) only observe masers with positive radial velocities and hence do not detect the masers we identify toward the central region of the UC HII region or those that trace the reversal in magnetic field polarity in G5.89-S.

Each of the 1612 MHz masers is seen in both RCP and LCP. Following the same procedure described for the 1667 MHz masers, we find that the velocity splitting between the different polarizations is greater than the velocity centroiding error for only one of the masers (feature number 3). The velocity splitting is 0.13 km s^{-1}, which is only $\simeq$15% of the linewidth. The B-field suggested by the pair is -1.05 mG; however, we note that the Zeeman splitting theory changes significantly when the velocity splitting between polarizations

is much less than a linewidth, so this value should be considered very uncertain.

3.3. Comparison with Methanol and Water Masers

Methanol (Kurtz et al. 2004) and water (Hofner & Churchwell 1996) masers have also been detected toward G5.89. The methanol masers do not appear to be associated with the main-line OH masers. While the 1667 MHz and 1612 MHz OH masers are nearly all projected toward the UC HII region, the methanol masers are offset ∼10 arcseconds N of the center of the UC HII region, with radial velocities ranging between 2.88 km s^{-1} and 15.48 km s^{-1}. The distribution of water masers is primarily elongated NE-SW. Two H_2O features are located along the E edge of the UC HII region with similar radial velocities as the 1667 MHz OH masers in the same region, suggesting a possible association.

4. Discussion

Previous authors have suggested that the main-line OH masers trace a rapidly expanding bipolar outflow (Zijlstra et al. 1990; Wood 1993). If they do trace an outflow, we would expect the spatial distribution and velocity structure of the masers to resemble that of the outflowing gas.

The 1667 MHz OH masers in G5.89 S and G5.89 Center are elongated primarily along a NE-SW axis (PA=82°) similar to the SiO outflow (Sollins et al. 2004), but are confined to an area ≃3 times smaller than that covered by SiO emission. We do not find a continuous velocity gradient along this axis, in contrast to the observations of Zijlstra et al. (1990). Further, the outflow structure suggested by Zijlstra et al. (1990) (northern outflow cone pointed toward Earth and southern cone pointing away) is of opposite orientation to the SiO outflow, where the peak in the red-shifted lobe is located NE of the blue-shifted emission.

The factors listed above do not rule out the possibility that the OH masers trace a bipolar outflow. The confinement of OH masers to the face of the UC HII region can be explained if the excitation conditions for OH masers only exist very close to the base of the outflow, as suggested by Zijlstra et al. (1990), while differences between the SiO(5-4) outflow and the outflowing gas traced by the OH masers could simply be due to the molecules tracing different components of the gas. However, we suggest that a simpler explanation may be that the OH masers are confined to the postshock region at the interface of the ionized gas shell and the ambient molecular material, similar to the models discussed in Elitzur & de Jong (1978).

The ionized gas appears to be expanding supersonically into the surrounding medium with an expansion velocity of 35 km s^{-1} (Acord et al. 1998). In the idealized case of expansion of a neutral shell, we would expect all features projected on the ionized shell to be blueshifted with respect to the systemic velocity of the UC HII region. Redshifted features would not appear projected near the central regions because the UC HII region is optically thick at 18 cm. Those features located at or close to the edge of the UC HII region should have radial velocities comparable to the systemic velocity of the central source.

Both of the above predicted characteristics are observed toward G5.89. All masers projected in the central region of G5.89 are blueshifted by 30-42 km s^{-1} with respect to the assumed systemic velocity of 10 km s^{-1}, consistent with the expansion velocity of the UC HII region, while maser emission projected on the edges of the UC HII region exhibits radial velocities close to the systemic velocity.

If the masers do trace an expanding UC HII region, we would expect to observe large proper motions between masers located along the edges of the UC HII region and very small proper motions for masers in the center of the UC HII region. At present, we only have relative proper motion measurements for masers along the edges of G5.89-E and G5.89-S. The relative motions of these features do suggest that the masers are moving away from each other at high speeds (20-30 km s^{-1}); however, such high expansion speeds are also consistent with a scenario in which the masers trace an outflow. A more definitive test awaits the determination of the tangential velocities of masers projected on the center of G5.89.

The observed magnetic field structure may also be naturally explained in the context of a neutral shell shocked by the expanding HII region. The ambient molecular gas surrounding G5.89 has a density of $\simeq 1.2\times10^5$ cm^{-3} (Cesaroni et al. 1991). The resulting Alfven speed, $v_A \simeq 2$ km s^{-1}, is significantly less than the expansion speed of the UC HII region (35 km s^{-1}), indicating that there is significantly more energy in expansion than in the B-field. Hence, the magnetic field will be swept up and expand along with the ionized gas shell. An expanding shell carrying a magnetic field will have polarity changes on the scale of the shell due to its curvature. For example, a magnetic field that is initially directed N in the plane of the sky with no component along the line of sight will develop a positive line-of-sight component above the center of expansion and a negative line-of-sight component below the expansion center after being swept up in the expanding ionized shell. This effect may explain the change in polarity observed between the southernmost masers in G5.89 South and those located several arcseconds N in G5.89 East and G5.89 Center. An illustration of the effect is presented in Bourke et al. (2001). The small-scale magnetic field reversal observed in G5.89 South (Figure 10) may arise if the expanding shell crosses the path of a clump of gas in the ambient medium. In this case a field reversal would occur on the clump size-scale. This

hypothesis is supported by the presence of a foreground molecular cloud to the southwest of the UC HII region traced in 1.3 mm continuum by Feldt et al. (1999) and in 350 μm continuum by Mueller et al. (2002).

5. Conclusions

The large number (>50) and velocity range ($\simeq$50 km s^{-1}) of 1667 MHz OH masers toward G5.89 distinguishes this region from other massive star formation regions with OH masers. While it has been previously suggested that the OH masers trace a rapidly expanding bipolar outflow, we suggest that the maser emission may alternatively arise in the dense postshock region at the interface of the supersonically expanding UC HII region and the ambient molecular cloud.

We identify 23 Zeeman pairs which indicate the presence of $\lesssim 2$ mG magnetic fields. An ordered reversal in magnetic field direction is present in the S region of G5.89. While the geometry hints at a toroidal pattern indicative of a dense disk-like structure, the distribution and velocity field of the OH masers suggests that this configuration is likely not the case. The field reversal could alternatively be explained if the expanding shell of ionized gas sweeps up the magnetic field lines and crosses the path of a neutral clump, thereby imprinting a field reversal on the clump size-scale.

We thank the referee for helpful comments that improved the quality of the paper. D.P.S. thanks Debra Shepherd and Christer Watson for useful discussions. *Facility: VLBA*

REFERENCES

Acord, J. M., Churchwell, E., & Wood, D. O. S. 1998, ApJ, 495, L107

Acord, J. M., Walmsley, C. M., & Churchwell, E. 1997, ApJ, 475, 693

Argon, A. L., Reid, M. J., & Menten, K. M. 2000, ApJS, 129, 159

Bourke, T. L., Myers, P. C., Robinson, G., & Hyland, A. R. 2001, ApJ, 554, 916

Cesaroni, R., Walmsley, C. M., Koempe, C., & Churchwell, E. 1991, A&A, 252, 278

Cook, A. H. 1968, MNRAS, 140, 299

Elitzur, M., & de Jong, T. 1978, A&A, 67, 323

Feldt, M., et al. 2003, ApJ, 599, L91

Feldt, M., Stecklum, B., Henning, T., Launhardt, R., & Hayward, T. L. 1999, A&A, 346, 243

Fish, V. L., & Reid, M. J. 2006, ApJS, 164, 99

Fish, V. L., Reid, M. J., Argon, A. L., & Zheng, X.-W. 2005, ApJS, 160, 220

Fish, V. L., Reid, M. J., Wilner, D. J., & Churchwell, E. 2003, ApJ, 587, 701

Gomez, Y., Rodriguez, L. F., Garay, G., & Moran, J. M. 1991, ApJ, 377, 519

Harvey, P. M., & Forveille, T. 1988, A&A, 197, L19

Harvey, P. M., Lester, D. F., Colome, C., Smith, B., Monin, J.-L., & Vauglin, I. 1994, ApJ, 433, 187

Hofner, P., & Churchwell, E. 1996, A&AS, 120, 283

Hutawarakorn, B., & Cohen, R. J. 1999, MNRAS, 303, 845

Hutawarakorn, B., & Cohen, R. J. 2003, MNRAS, 345, 175

Hutawarakorn, B., & Cohen, R. J. 2005, MNRAS, 357, 338

Hutawarakorn, B., Cohen, R. J., & Brebner, G. C. 2002, MNRAS, 330, 349

Kurtz, S., Hofner, P., & Álvarez, C. V. 2004, ApJS, 155, 149

Moran, J. M., Reid, M. J., Lada, C. J., Yen, J. L., Johnston, K. J., & Spencer, J. H. 1978, ApJ, 224, L67

Mueller, K. E., Shirley, Y. L., Evans, N. J., II, & Jacobson, H. R. 2002, ApJS, 143, 469

Reid, M. J., Haschick, A. D., Burke, B. F., Moran, J. M., Johnston, K. J., & Swenson, G. W. 1980, ApJ, 239, 89

Reifenstein, E. C., Wilson, T. L., Burke, B. F., Mezger, P. G., & Altenhoff, W. J. 1970, A&A, 4, 357

Shu, F., Najita, J., Ostriker, E., Wilkin, F., Ruden, S., & Lizano, S. 1994, ApJ, 429, 781

Sollins, P. K., et al. 2004, ApJ, 616, L35

Turner, B. E. 1969, AJ, 74, 985

Uchida, Y., & Shibata, K. 1985, PASJ, 37, 515

Watson, C. 2004, Ph.D. Thesis

Wood, D. O. S. 1993, in ASP Conf. Ser. 35: Massive Stars: Their Lives in the Interstellar Medium, 108

Wood, D. O. S., & Churchwell, E. 1989, ApJS, 69, 831

Zijlstra, A. A., Pottasch, S. R., Engels, D., Roelfsema, P. R., Hekkert, P. T.-L., & Umana, G. 1990, MNRAS, 246, 217

Table 1. Summary of Observations

OH Line	RA (2000)	Dec (2000)	Bandwidth (MHz)	Spec. Res. (km s^{-1})	Beam Size (mas)	Beam PA (°)	Noise (mJy $beam^{-1}$)
1667	18:00:30.3820	−24:04:00.825	1.0	0.22	45 × 15	27	49
1612	18:00:30.3820	−24:04:00.825	1.0	0.21	20 × 7	7	129

Table 2. G5.886−0.393 1667 MHz LCP Maser Parameters

Maser Feature	$\Delta\alpha$ (mas)	$\Delta\delta$ (mas)	Vel. (km s^{-1})	Δv (km s^{-1})	Flux Density (Jy)
1	−628	−2857	15.29	0.30	0.66
2	−566	−2966	14.51	0.39	0.51
3	−549	−2733	14.68	0.50	0.55
4	−519	−2803	14.09	0.85	0.70
5	−517	−2867	15.30	0.40	0.47
6	−514	−2648	14.02	0.45	1.34
7	−513	−2706	14.50	0.29	2.05
8	−492	−2745	13.78	0.41	0.91
9	−428	−2677	11.38	0.55	0.64
10	−421	−2517	13.36	0.38	4.62
11	−399	−2491	13.15	0.96	0.60
12	−382	−1862	−20.41	0.48	0.79
13	−371	−232	−28.17	0.54	0.49
14	−365	−1659	−18.20	0.63	1.99
15	−339	−2687	15.17	0.57	0.54
16	−287	−1702	−18.83	0.50	7.20
17	−285	−1775	−21.08	0.42	2.85
18	−285	1	−31.53	0.47	0.91
19	−273	−1734	−20.41	0.33	4.22
20	−225	−1802	−22.19	0.48	2.50
21	−183	13	−29.33	0.43	2.09
22	−182	−2006	−28.86	0.77	0.92
23	−180	−425	−22.03	0.59	0.55
24	−162	−440	−21.37	0.55	0.63
25	−139	−1991	−26.98	1.14	0.69
26	−122	−1820	−20.80	0.62	1.09
27	−121	−1990	−26.37	0.57	2.80
28	−111	−131	−29.66	0.36	2.16
29	−96	−1810	−20.13	0.47	0.66
30	−86	−102	−29.14	0.53	1.55
31	−38	−1812	−19.22	0.45	9.80
32	−34	−267	−25.56	0.35	3.77
33	−5	−1790	−17.92	0.51	3.40
34	118	−287	−24.67	0.27	1.56
35	232	−261	−26.82	0.42	1.11
36	260	−292	−25.91	0.27	0.77
37	291	−313	−25.13	0.35	4.30
38	318	−293	−25.96	0.33	1.42
39	329	−430	−23.15	0.48	1.86
40	362	−1481	−18.32	0.46	0.68
41	378	−314	−26.82	0.34	2.93
42	395	−350	−26.11	0.56	2.71
43	476	−1303	−24.49	0.41	0.60
44	497	−569	−23.00	0.57	0.58
45	566	259	−31.17	0.78	1.78

Table 2—Continued

Maser Feature	$\Delta\alpha$ (mas)	$\Delta\delta$ (mas)	Vel. (km s^{-1})	Δv (km s^{-1})	Flux Density (Jy)
46	616	282	−32.13	0.38	0.78
47	626	−1188	−24.37	0.34	0.71
48	657	−1156	−23.13	0.46	0.82
49	1016	343	−26.95	0.67	1.69
50	1017	214	−24.12	0.33	0.61
51	1028	311	−26.29	0.38	2.36
52	2128	−778	−29.88	0.34	1.01
53	2221	−183	−11.74	0.36	0.63
54	2756	−402	−15.05	0.33	2.93
55	2829	−425	−16.67	0.45	7.50
56	3342	−1980	11.02	0.32	0.81
57	3369	−768	8.33	0.34	0.34
58	3410	−760	8.92	0.32	0.44
59	3470	−686	9.78	0.27	6.22

Table 3. G5.886−0.393 1667 MHz RCP Maser Parameters

Maser Feature	$\Delta\alpha$ (mas)	$\Delta\delta$ (mas)	Vel. (km s^{-1})	Δv (km s^{-1})	Flux Density (Jy)
1	−626	−2858	15.19	0.34	1.52
2	−530	−2813	14.29	0.23	0.81
3	−516	−2801	13.74	0.58	1.34
4	−495	−2668	14.27	0.31	0.44
5	−485	−2699	14.59	0.32	0.56
6	−474	−2585	11.52	0.43	0.30
7	−442	−2795	14.51	0.28	0.24
8	−428	−2678	11.37	0.59	0.38
9	−421	−309	−26.76	0.39	0.87
10	−420	−2468	11.87	0.48	0.47
11	−415	−2510	12.66	0.38	0.50
12	−389	−2768	7.96	0.42	0.21
13	−380	−1863	−19.72	0.44	0.99
14	−366	−228	−28.10	0.57	1.20
15	−356	−2695	15.20	0.26	0.42
16	−339	−2546	7.04	0.68	0.46
17	−299	−2641	7.05	0.43	0.64
18	−285	−7	−31.61	0.40	1.18
19	−275	−1695	−18.65	0.65	2.79
20	−270	−1737	−19.95	0.33	1.53
21	−269	−197	−28.50	0.25	0.63
22	−242	−328	−25.15	0.35	0.92
23	−218	−1799	−21.97	0.47	0.98
24	−214	−5	−29.72	0.35	1.49
25	−184	−2005	−29.23	0.67	1.09
26	−184	16	−29.34	0.35	2.03
27	−141	−1996	−27.53	0.94	0.72
28	−126	−132	−29.64	0.29	1.25
29	−122	−1987	−26.86	0.78	1.15
30	−120	−1819	−21.04	0.62	1.27
31	−100	−260	−26.56	0.43	0.90
32	−95	−1808	−20.38	0.47	1.12
33	−92	−121	−29.57	1.24	0.64
34	−86	−103	−29.16	0.51	1.05
35	−62	−153	−30.27	0.30	0.47
36	−32	−266	−25.33	0.49	2.41
37	−16	−239	−28.49	0.28	0.81
38	−5	−1781	−18.16	0.40	2.73
39	55	−236	−26.87	0.29	0.51
40	223	−444	−20.60	0.37	0.68
41	235	−270	−26.54	0.36	0.67
42	286	−309	−25.10	0.30	0.64
43	333	−430	−22.86	0.42	1.70
44	380	−310	−26.61	0.31	0.70
45	476	−1301	−23.97	0.39	0.55

Table 3—Continued

Maser Feature	$\Delta\alpha$ (mas)	$\Delta\delta$ (mas)	Vel. (km s^{-1})	Δv (km s^{-1})	Flux Density (Jy)
46	498	−572	−22.52	0.46	0.65
47	568	266	−31.48	0.79	2.61
48	1018	339	−26.84	0.50	3.31
49	1039	308	−26.14	0.36	0.90
50	2111	−779	−30.09	0.30	0.77
51	2253	−201	−11.54	0.38	0.99
52	2758	−401	−14.86	0.31	1.73
53	2821	−276	−16.35	0.42	0.65
54	2825	−426	−16.20	0.49	2.65
55	3473	−685	10.28	0.22	4.88

Table 4. G5.886−0.393 1612 MHz Maser Parameters

Maser Feature	$\Delta\alpha$ (mas)	$\Delta\delta$ (mas)	Vel. (km s^{-1})	Δv (km s^{-1})	Flux Density (Jy)
1612 MHz LCP					
1	−181	109	−19.26	0.65	3.30
2	−157	163	−20.51	0.87	2.26
3	0	0	−21.31	0.85	12.05
1612 MHz RCP					
1	−179	106	−19.37	0.84	4.63
2	−157	159	−20.43	0.80	2.73
3	0	0	−21.43	1.00	12.39

Table 5. Zeeman Pairs

RCP			LCP				Separation	
$\Delta\alpha$ (mas)	$\Delta\delta$ (mas)	Velocity (km s^{-1})	$\Delta\alpha$ (mas)	$\Delta\delta$ (mas)	Velocity (km s^{-1})	B (mG)	Ang. (mas)	Lin. (AU)
−516	−2801	13.74	−519	−2803	14.09	−0.96	4.16	8.32
−415	−2510	12.66	−421	−2517	13.36	−1.97	8.53	17.07
−380	−1863	−19.72	−382	−1862	−20.41	1.94	1.82	3.65
−276	−1695	−18.65	−287	−1702	−18.83	0.51	13.62	27.25
−270	−1737	−19.95	−273	−1734	−20.41	1.29	4.39	8.78
−218	−1799	−21.97	−225	−1802	−22.19	0.62	7.46	14.93
−184	−2005	−29.23	−182	−2006	−28.86	−1.05	1.85	3.70
−141	−1996	−27.53	−139	−1991	−26.98	−1.57	5.37	10.73
−122	−1987	−26.86	−121	−1990	−26.37	−1.37	2.74	5.48
−120	−1819	−21.04	−122	−1820	−20.80	−0.67	2.11	4.23
−32	−266	−25.33	−34	−267	−25.56	0.65	2.44	4.88
−5	−1781	−18.16	−5	−1790	−17.92	−0.68	8.98	17.96
235	−270	−26.54	232	−261	−26.82	0.81	8.84	17.68
333	−430	−22.86	329	−430	−23.15	0.83	3.57	7.14
380	−310	−26.61	378	−314	−26.82	0.59	4.45	8.89
476	−1301	−23.97	476	−1303	−24.49	1.49	2.25	4.50
498	−572	−22.52	497	−569	−23.00	1.35	3.20	6.40
568	266	−31.48	566	259	−31.17	−0.88	7.03	14.06
1018	339	−26.84	1016	343	−26.95	0.29	5.14	10.28
1039	308	−26.14	1028	311	−26.29	0.45	10.57	21.14
2758	−401	−14.86	2756	−402	−15.05	0.52	1.86	3.72
2825	−426	−16.20	2829	−425	−16.67	1.34	4.31	8.63
3473	−685	10.28	3470	−686	9.78	1.41	3.14	6.28

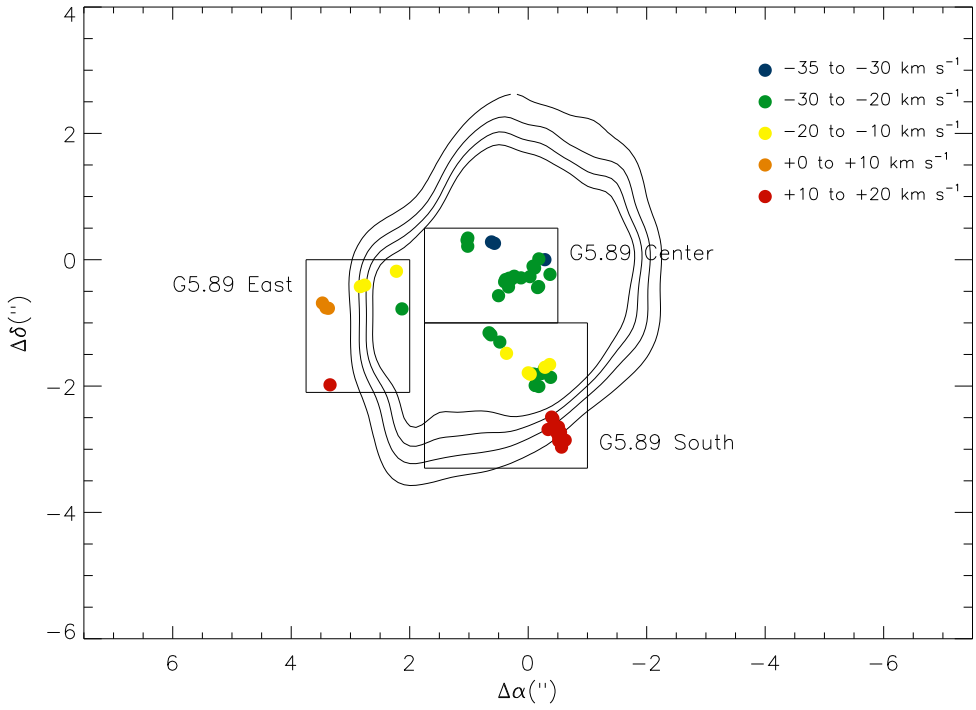

Fig. 1.— Left Circular Polarized 1667 MHz OH masers overlaid on 8.5 GHz continuum. The origin corresponds to α_{2000}=$18^h00^m30\overset{s}{.}382$ δ_{2000}=$-24°04'00\overset{''}{.}829$. The 8.5 GHz continuum data was obtained with the VLA in AB configuration (Churchwell 2003, private communication) and has a beam size of 0.6×0.5 arcseconds. The contour levels of the radio continuum image are 0.03, 0.06, 0.10, 0.13 Jy beam^{-1}.

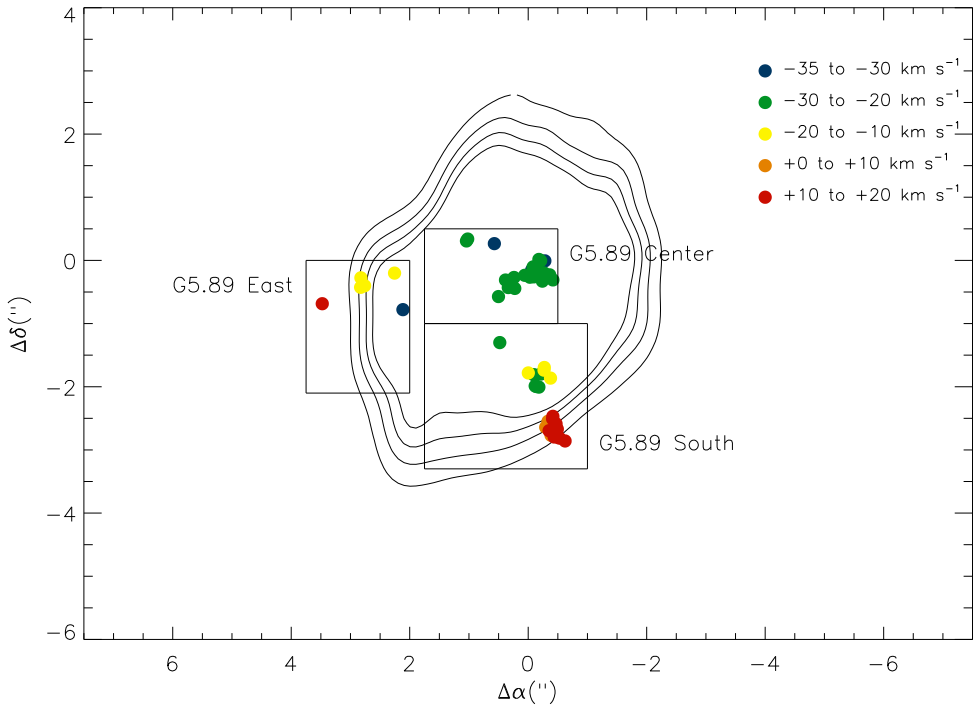

Fig. 2.— Right Circular Polarized 1667 MHz OH masers overlaid on 8.5 GHz continuum. See Figure 1 for details.

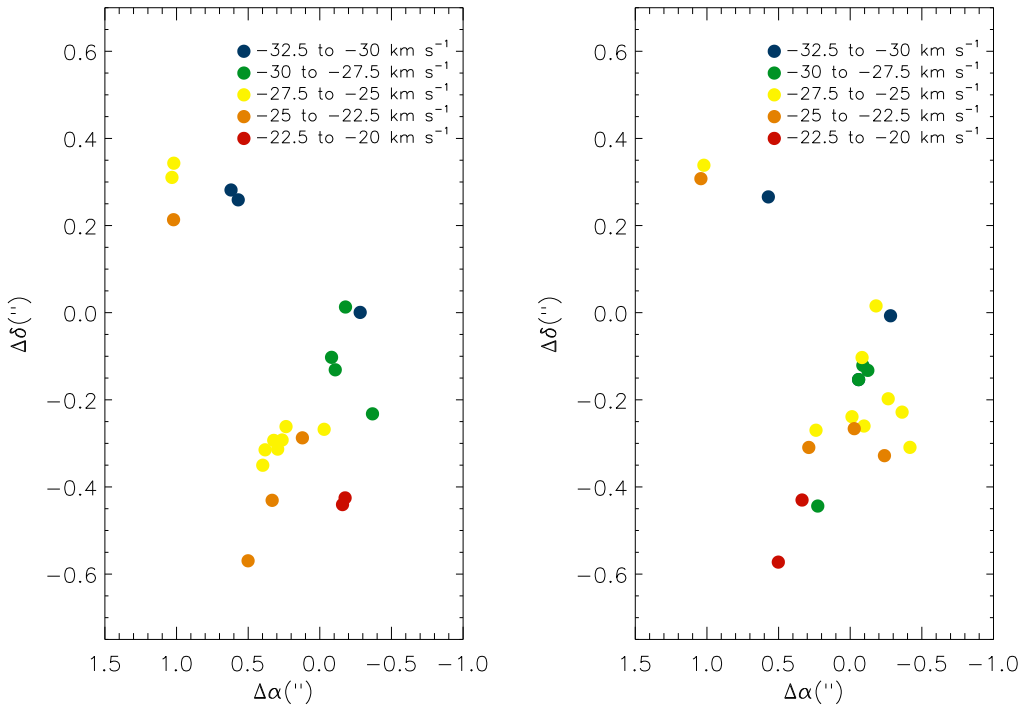

Fig. 3.— Left: Positions of LCP 1667 MHz masers in G5.89 Center. Right: Positions of RCP 1667 MHz masers in G5.89 Center. See Figure 1 for details.

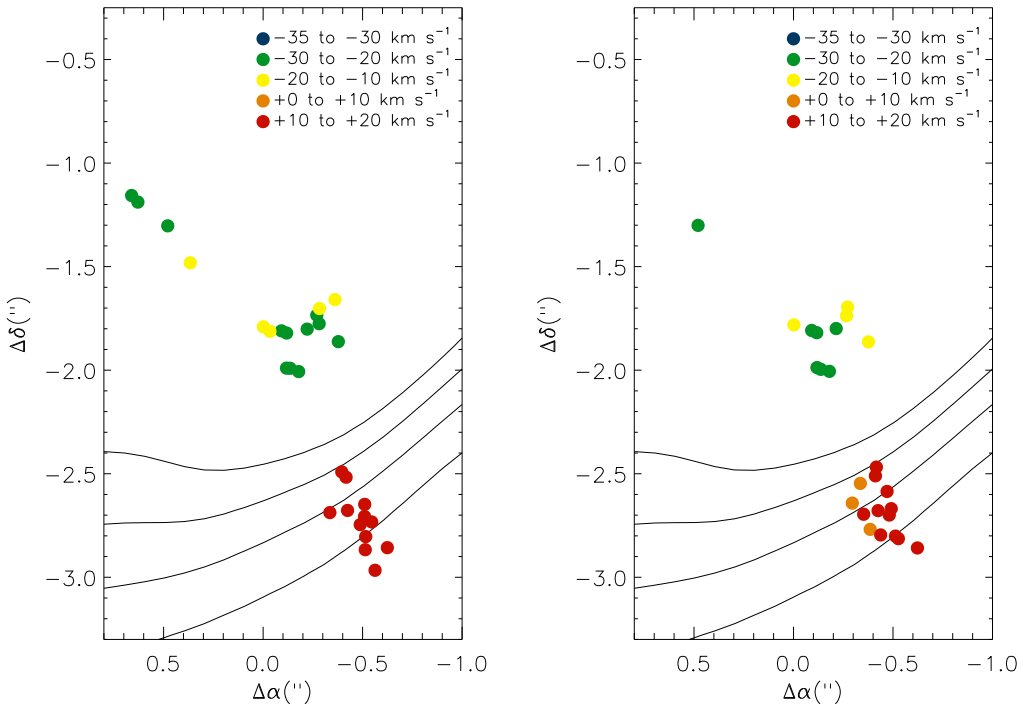

Fig. 4.— Left: Positions of LCP 1667 MHz masers in G5.89 South. Right: Positions of RCP 1667 MHz masers in G5.89 South. See Figure 1 for details.

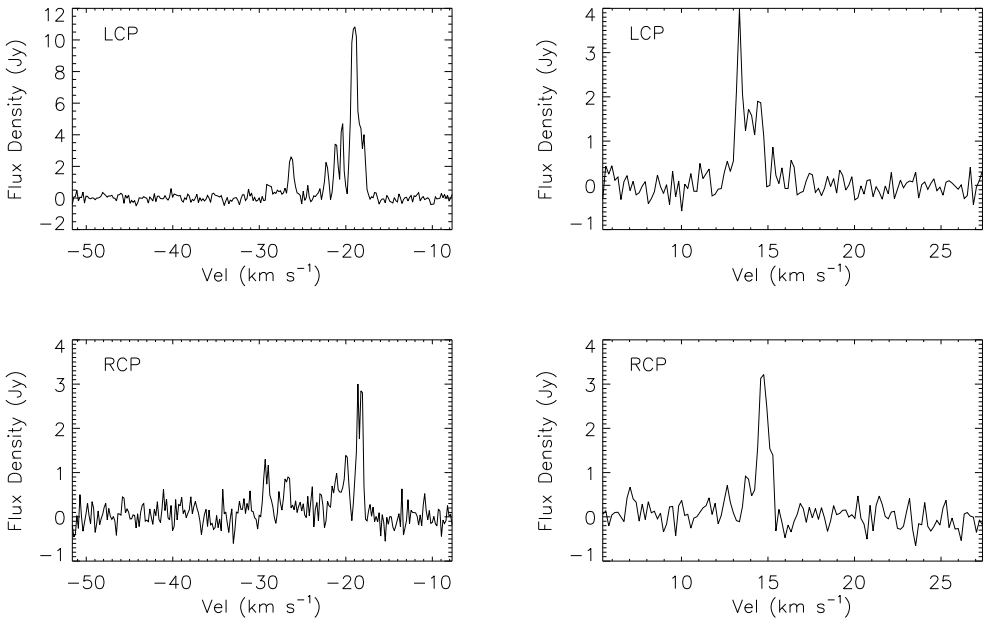

Fig. 5.— Spectrum of 1667 MHz emission averaged over S region as specified in Figure 1. The LCP spectra is displayed in the top panel and the RCP spectrum is displayed in the bottom panel. The beam size is 45×15 mas at 1667 MHz. Velocities are with respect to the local standard of rest. Line emission from OH masers spans 45 km s^{-1} in a region 1.8x1.4 arcseconds in size.

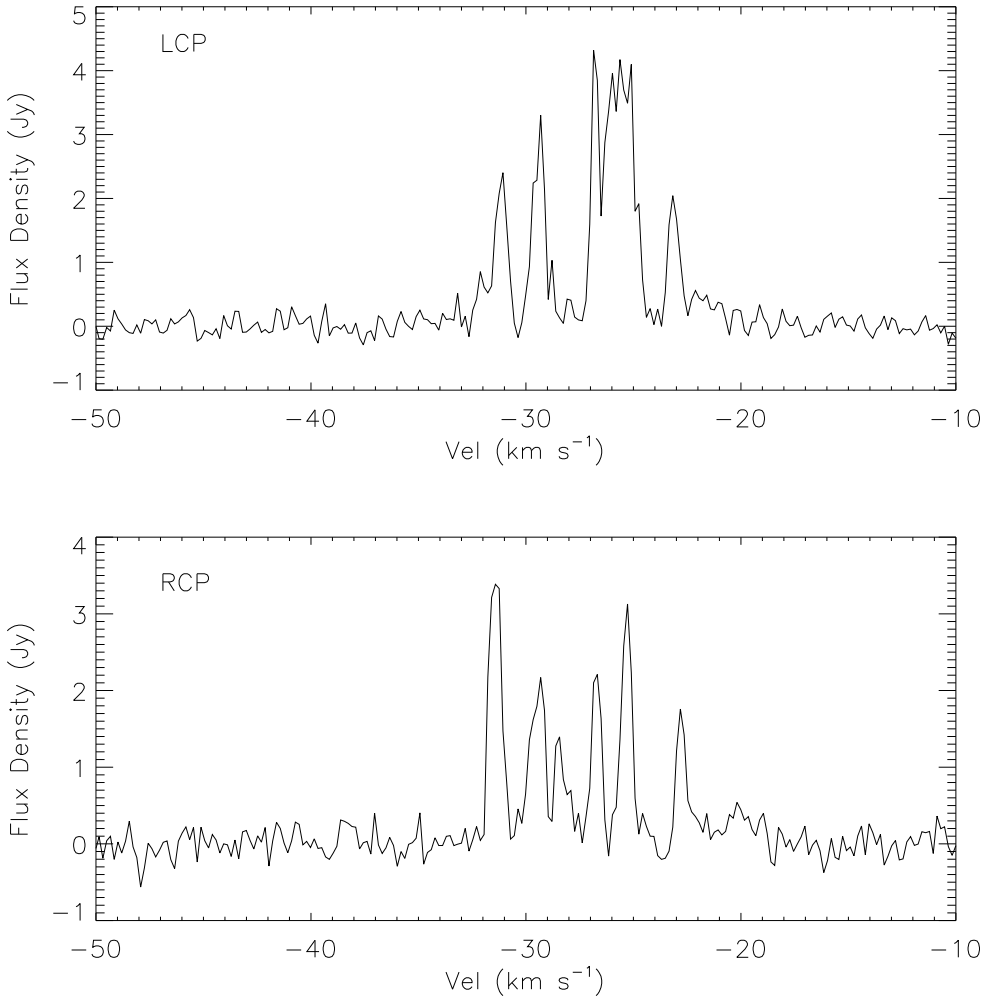

Fig. 6.— Spectrum of 1667 MHz emission averaged over the central region of G5.89 (see Fig 1). The LCP spectra is displayed in the top panel and the RCP spectrum is displayed in the bottom panel. The beam size is 45×15 mas at 1667 MHz. Masers are only detected in this region at negative LSR velocities.

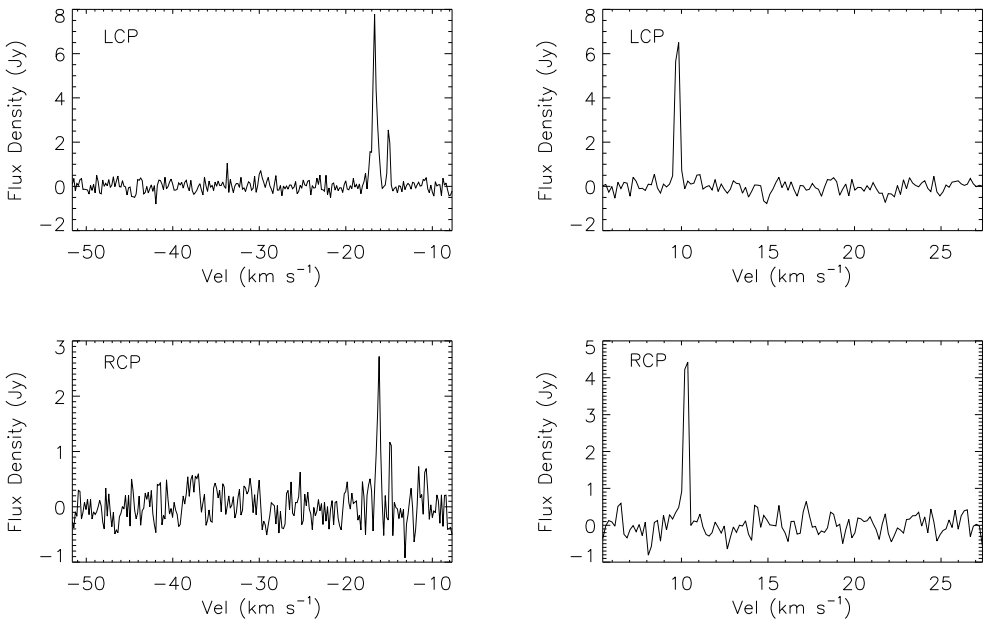

Fig. 7.— Spectra of LCP 1667 MHz emission averaged over E region of G5.89 (see Fig. 1). The LCP spectra is displayed in the top panel and the RCP spectrum is displayed in the bottom panel. The beam size is 45×15 mas at 1667 MHz.

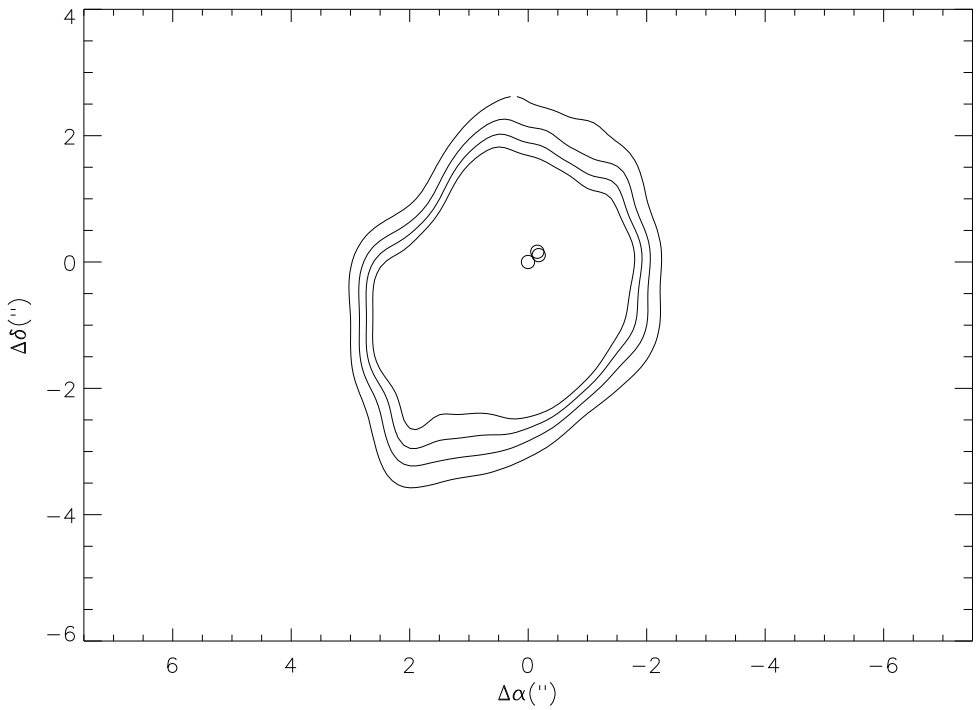

Fig. 8.— Left Circular Polarized 1612 MHz OH masers overlaid on 8.5 GHz continuum. The beam size is 20×7 mas at 1612 MHz.

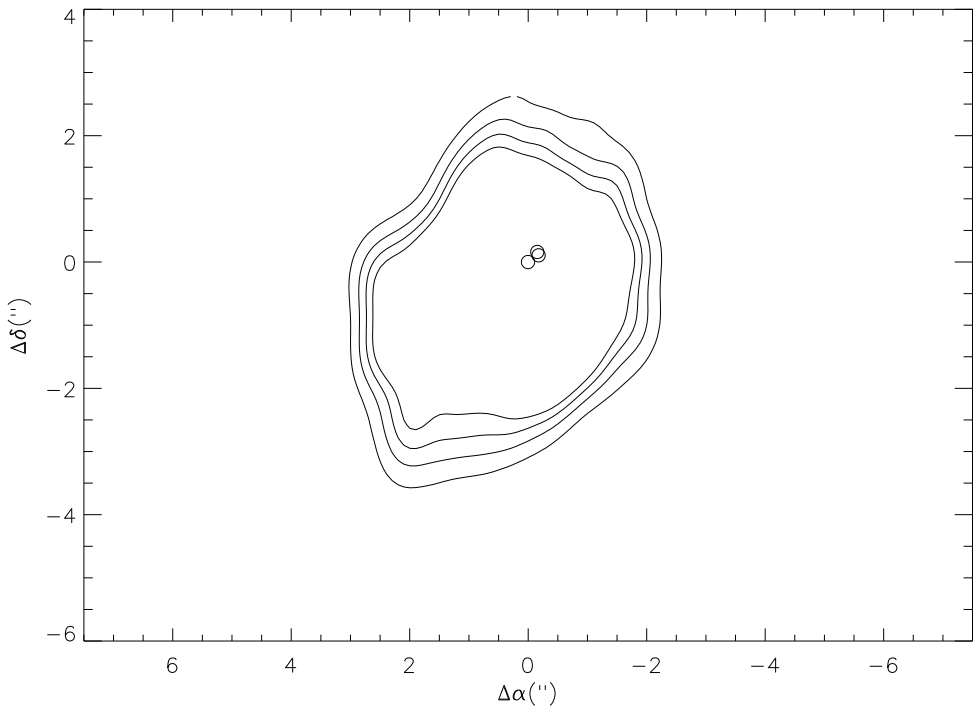

Fig. 9.— Right Circular Polarized 1612 MHz OH masers overlaid on 8.5 GHz continuum. The beam size is 20×7 mas at 1612 MHz.

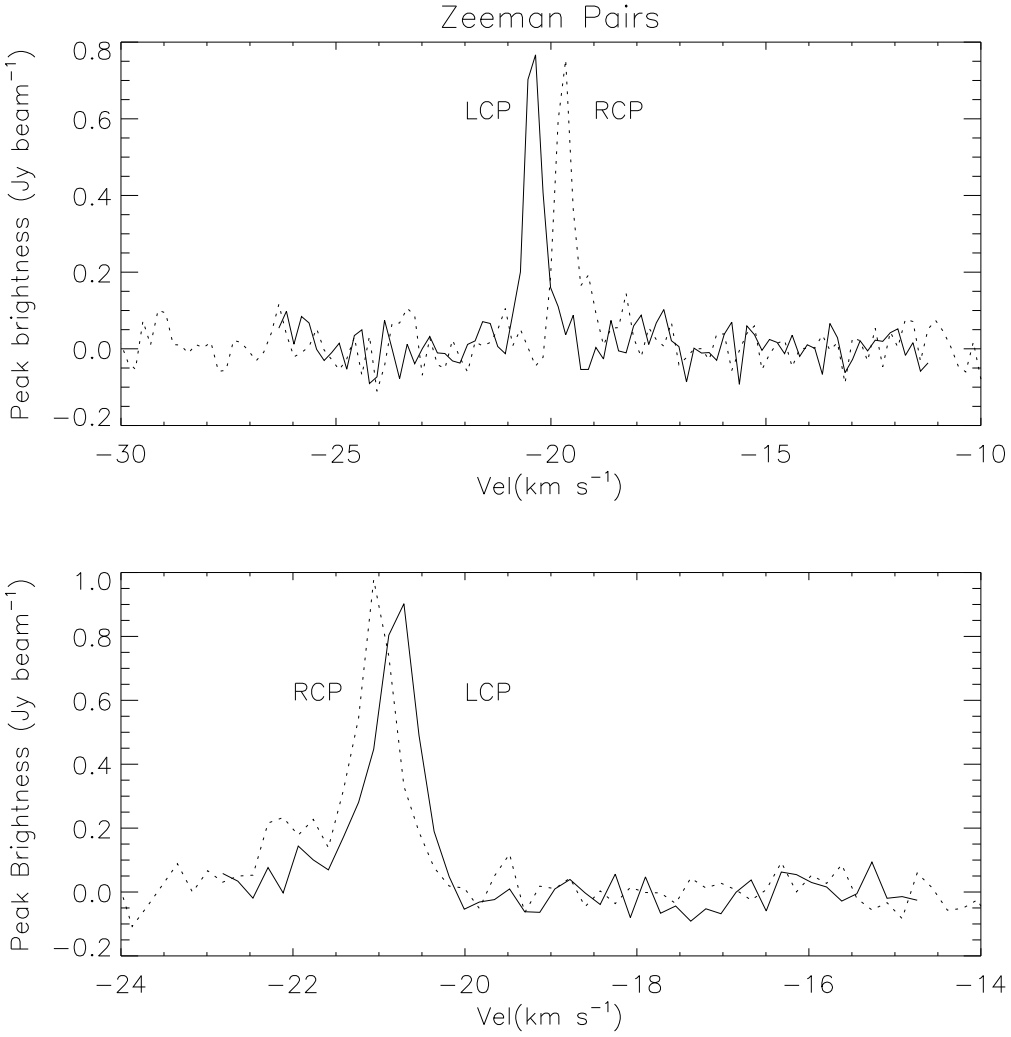

Fig. 10.— VLBA spectra of two typical Zeeman pairs at 1667 MHz in both LCP and RCP.

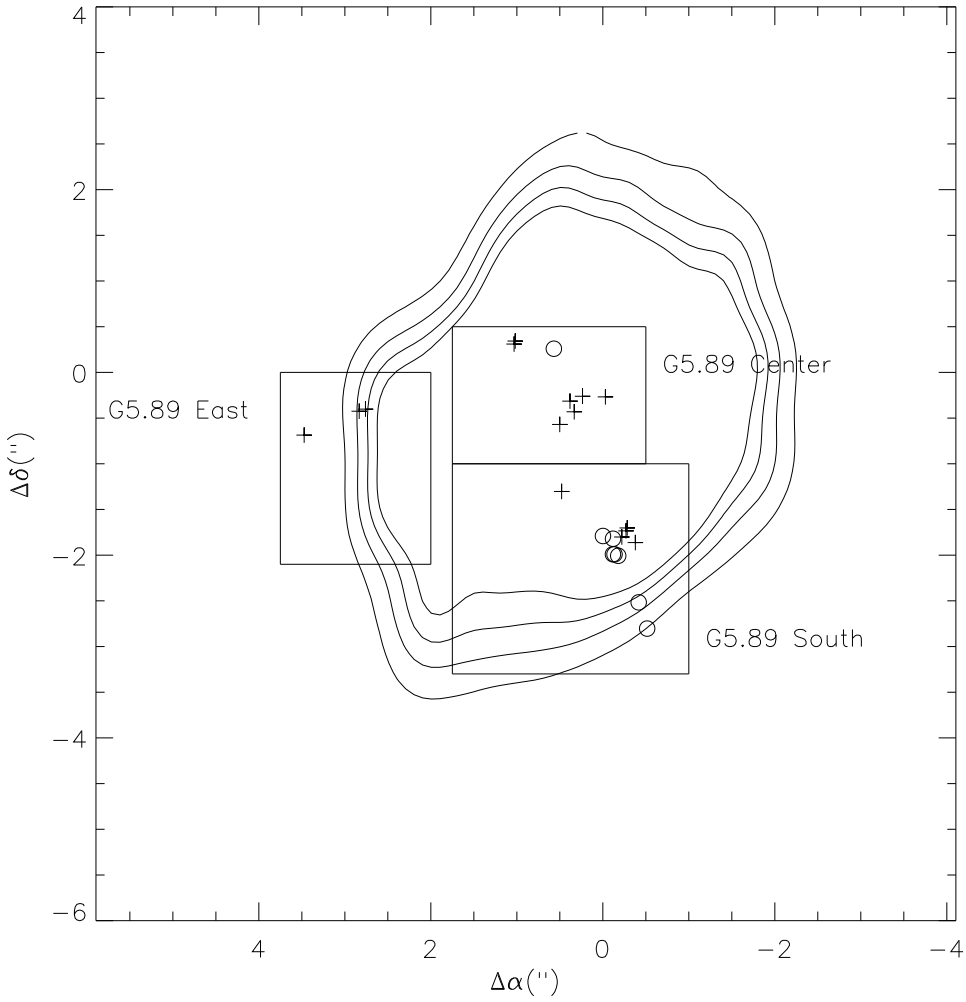

Fig. 11.— Zeeman Pairs identified toward G5.89 at 1667 MHz overlaid over 8.5 GHz continuum emission. Circles are representive of a negative magnetic field, whereas crosses indicate a positive B-field polarity.

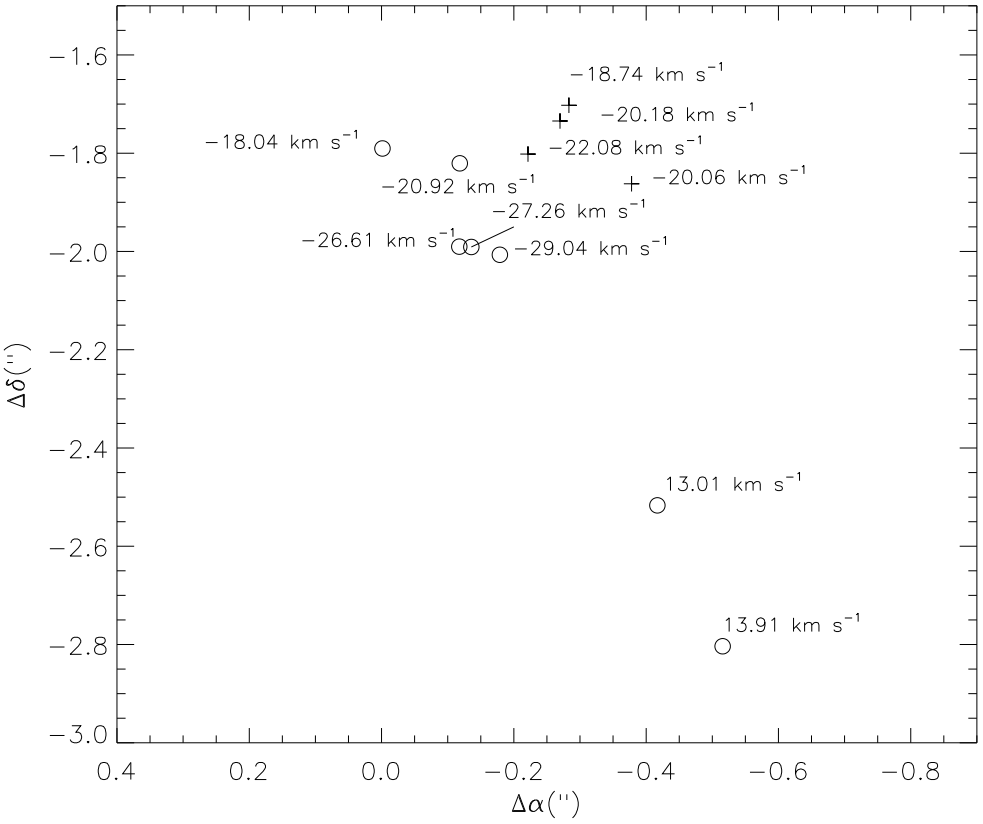

Fig. 12.— Magnetic-field structure in G5.89 South as traced by 1667 MHz OH masers determined using the VLBA of the NRAO. Circles are representative of a negative magnetic field, whereas crosses indicate a positive B-field polarity. Radial velocities (after correction for the Zeeman effect) are noted next to each feature. The direction of the magnetic field changes over $\simeq$0.3 arcseconds, corresponding to 600 AU at the distance of G5.89.